The Shape of Au_8: Gold Leaf or Gold Nugget? - SUPPORTING INFORMATION

Stefano A. Serapian[1], Michael J. Bearpark[1], and Fernando Bresme[1,2]

[1]Imperial College, London, SW7 2AZ, U. K.
[2]Department of Chemistry, Norwegian University of Science and Technology, Trondheim, Norway

May 11, 2013

Vibrational Frequencies

Tables S1-S4 below summarize the vibrational frequencies of the four Au_8 isomers considered, as predicted by all of the methods employed except CCSD(T). Resulting infrared (IR) spectral predictions vary considerably from method to method, both in terms of peak intensity and peak ratio, especially for the nugget isomers (and especially for **F8**): formatted *Gaussian09* checkpoint files for these calculations may be obtained electronically.

Table S1: Vibrational frequencies predicted for Au_8 **F2**

Method	**Calculated Vibrational Frequencies / cm^{-1}**																	
PBE/LANL2DZ	3.92	12.25	32.19	34.74	35.20	37.94	53.38	56.49	57.93	76.99	91.75	95.93	96.40	118.89	129.19	173.07	173.52	194.83
PBE/SBKJC(*1f*)	2.70	8.22	31.50	33.08	33.44	37.27	56.28	59.82	60.98	78.65	96.72	98.65	98.82	122.39	135.90	175.85	176.72	196.83
M06-L/LANL2DZ	6.05	14.53	29.76	32.64	36.05	39.28	53.89	57.24	62.86	80.01	88.76	101.22	101.91	123.26	134.77	174.02	175.99	193.67
M06-L/SBKJC(*1f*)	2.84	24.02	30.20	32.06	34.68	35.07	46.58	52.25	72.87	78.59	96.81	101.90	103.31	124.58	137.71	169.49	181.65	193.72
B2PLYP/LANL2DZ	1.98	17.21	30.61	33.79	33.93	37.47	53.28	58.21	58.39	76.54	89.87	97.39	97.43	118.32	126.99	169.84	170.16	190.88
B2PLYP/SBKJC(*1f*)	0.91	20.05	32.14	33.32	33.52	37.21	57.27	63.64	63.71	81.04	98.27	102.59	102.71	126.02	138.07	179.91	180.12	200.93
B2PLYP/MWB60	3.35	20.05	31.07	33.81	34.02	39.01	56.11	60.93	61.09	78.63	94.31	100.66	100.70	122.46	134.57	175.72	176.00	196.91
B2PLYP/cc-pVTZ-PP	2.85	14.08	33.64	36.30	36.40	39.99	58.51	63.35	63.43	83.40	99.69	104.67	104.76	128.39	141.20	183.62	183.79	204.57
MP2/SBKJC(*1f*)	6.84	19.84	32.89	33.89	33.90	34.49	72.49	77.81	77.83	90.00	117.31	119.14	119.16	145.53	158.65	206.82	206.82	230.95

Table S2: Vibrational frequencies predicted for Au_8 **F5**

Method	**Calculated Vibrational Frequencies / cm^{-1}**																	
PBE/LANL2DZ	19.75	20.68	49.67	49.90	49.95	69.41	69.90	70.04	73.27	73.86	73.90	81.15	97.62	97.99	135.83	135.99	136.46	137.89
PBE/SBKJC(*1f*)	19.55	20.51	49.60	49.78	50.63	72.30	72.73	73.81	80.51	81.89	82.24	82.26	103.01	103.89	140.55	140.90	141.25	141.40
M06-L/LANL2DZ	22.73	28.72	51.04	52.16	53.19	64.44	66.55	68.56	76.18	76.29	78.17	87.19	93.71	99.44	127.61	127.63	129.54	137.87
M06-L/SBKJC(*1f*)	25.10	29.36	52.72	53.15	53.98	70.39	71.85	73.67	78.46	79.14	80.70	88.53	98.33	102.82	130.83	131.46	132.59	142.17
B2PLYP/LANL2DZ	21.69	21.99	51.50	51.53	52.02	68.81	69.06	69.59	75.99	76.02	76.23	81.01	99.78	100.07	136.29	136.39	136.48	136.69
B2PLYP/SBKJC(*1f*)	19.11	19.68	50.67	50.74	51.77	73.00	73.05	73.98	82.26	84.61	84.71	84.79	107.37	107.76	145.74	145.86	145.97	146.04
B2PLYP/MWB60	21.36	21.79	51.56	51.61	51.70	70.60	70.98	71.01	80.32	80.37	80.45	82.08	102.81	103.01	140.11	140.17	140.32	140.82
B2PLYP/cc-pVTZ-PP	18.36	18.78	51.14	51.21	52.30	73.42	73.49	74.35	82.82	84.35	84.43	84.62	107.28	107.54	145.62	145.76	145.81	145.91
MP2/SBKJC(*1f*)	19.34	19.40	56.03	56.04	56.12	84.86	84.88	84.94	92.99	105.07	105.1	105.17	130.37	130.39	171.53	172.43	172.43	172.44

Table S3: Vibrational frequencies predicted for Au_8 **F6**

Method	**Calculated Vibrational Frequencies / cm^{-1}**																	
PBE/LANL2DZ	13.90	27.40	36.59	41.71	51.83	58.39	59.86	65.61	74.10	74.13	85.89	89.94	93.63	97.71	126.05	128.05	140.08	164.38
PBE/SBKJC(*1f*)	13.93	28.61	37.53	42.75	52.37	61.54	62.15	71.20	76.04	82.77	90.04	97.44	97.61	101.89	132.07	132.86	145.07	166.22
M06-L/LANL2DZ	23.00	35.58	42.67	46.69	59.62	60.98	61.39	63.87	70.38	83.21	84.01	87.88	96.60	102.22	120.89	122.13	134.27	165.09
M06-L/SBKJC(*1f*)	29.83	42.14	42.57	43.98	58.44	60.71	62.19	65.28	74.24	82.82	86.91	91.81	98.20	104.27	123.65	125.88	137.30	163.24
B2PLYP/LANL2DZ	13.95	27.69	37.86	41.21	52.60	56.49	61.42	68.94	74.67	75.53	86.73	90.25	94.08	97.62	124.35	128.13	139.83	162.93
B2PLYP/SBKJC(*1f*)	15.10	28.97	39.94	41.59	54.69	59.63	64.99	74.80	78.93	84.86	93.75	99.59	101.65	105.27	135.54	136.89	149.87	171.14
B2PLYP/MWB60	14.00	28.00	39.23	41.97	54.06	58.15	62.89	72.12	76.68	80.55	89.79	94.71	97.64	101.39	129.52	131.53	143.94	166.52
B2PLYP/cc-pVTZ-PP	9.50	27.21	38.31	44.06	53.36	63.88	64.88	75.66	79.62	85.47	93.23	99.90	101.26	104.76	136.30	138.58	151.06	173.74
MP2/SBKJC(*1f*)	25.19	35.93	44.82	48.59	62.48	67.72	74.76	88.95	94.85	103.00	112.58	119.63	123.95	125.29	156.86	161.55	175.00	200.98

Table S4: Vibrational frequencies predicted for Au_8 **F8**

Method	**Calculated Vibrational Frequencies / cm^{-1}**																	
PBE/LANL2DZ	26.57	31.54	35.97	46.98	51.88	51.88	58.11	62.90	62.90	63.49	92.54	92.76	92.76	101.29	126.75	126.75	136.65	140.33
PBE/SBKJC(*1f*)	34.70	37.47	38.97	52.36	52.61	52.61	62.92	63.77	63.77	69.54	94.48	98.25	98.25	107.93	130.11	130.11	140.37	144.84
M06-L/LANL2DZ	22.95	39.72	42.84	43.20	51.91	51.92	63.32	64.09	64.12	69.61	88.74	88.77	94.01	98.76	119.16	119.22	128.48	132.13
M06-L/SBKJC(*1f*)	29.04	39.37	46.95	50.74	52.39	52.39	65.06	65.06	70.52	74.43	92.11	92.11	95.43	104.75	121.56	121.56	131.56	134.77
B2PLYP/LANL2DZ	35.58	36.19	39.25	51.57	52.38	52.38	61.08	63.04	63.04	66.82	93.45	93.45	93.46	103.70	125.90	125.90	134.94	139.62
B2PLYP/SBKJC(*1f*)	36.40	41.97	45.51	54.64	54.65	57.76	63.46	66.47	66.47	76.29	99.69	102.63	102.63	112.86	134.43	134.43	144.91	149.79
B2PLYP/MWB60	36.36	38.63	42.53	53.49	53.49	55.74	61.87	64.76	64.76	71.60	96.13	97.88	97.88	107.76	129.04	129.04	138.87	143.74
B2PLYP/cc-pVTZ-PP	36.26	44.10	46.06	54.27	54.27	55.56	65.21	66.07	66.07	77.07	97.45	101.97	101.97	113.36	134.66	134.66	145.67	150.28
MP2/SBKJC(*1f*)	44.77	46.11	64.67	65.25	65.25	72.16	77.64	79.55	79.55	98.97	123.45	126.08	126.08	135.71	157.58	157.58	170.32	176.21

Vertical Detachment Energy

Table S5 below lists the vertical detachment energies ($Au_8 \rightarrow Au_8^+ + e^-$) for the four Au_8 isomers considered, as predicted by all of the methods employed except CCSD(T). A rough experimental upper limit of 8.65 eV is reported by Diefenbach and Kim,[1] referring to a 1992 study.[2]

Table S5: Vertical detachment energies predicted for Au_8 **F2**, **F5**, **F6** and **F8**

Method	**Vertical Detachment Energy / eV**			
	F2	**F5**	**F6**	**F8**
PBE/LANL2DZ	8.09	7.92	7.56	7.70
PBE/SBKJC(*1f*)	7.80	7.75	7.40	7.55
M06-L/LANL2DZ	7.69	7.65	7.18	7.41
M06-L/SBKJC(*1f*)	7.34	7.54	7.05	7.30
B2PLYP/LANL2DZ	7.86	7.80	7.38	7.54
B2PLYP/SBKJC(*1f*)	8.01	7.87	7.45	7.64
B2PLYP/MWB60	7.85	7.77	7.32	7.51
B2PLYP/cc-pVTZ-PP	8.13	7.97	7.58	7.74
MP2/SBKJC(*1f*)	8.44	8.46	7.92	8.27

Vertical Electron Affinity

Table S6 below lists the vertical electron affinities ($Au_8 + e^- \rightarrow Au_8^-$) for the four Au_8 isomers considered, as predicted by all of the methods employed except CCSD(T). From their photoelectron spectrum of Au_8^-, Häkkinen and co-authors[3] report a vertical detachment energy of 2.79 eV, implying a vertical electron affinity of −2.79 eV for neutral Au_8. This is in line with a previous 1992 study.[4]

Table S6: Vertical electron affinities predicted for Au_8 **F2**, **F5**, **F6** and **F8**

Method	**Vertical Electron Affinity / eV**			
	F2	**F5**	**F6**	**F8**
PBE/LANL2DZ	−2.82	−2.16	−2.36	−2.25
PBE/SBKJC(*1f*)	−2.70	−2.02	−2.28	−2.18
M06-L/LANL2DZ	−2.54	−1.96	−2.16	−2.10
M06-L/SBKJC(*1f*)	−2.41	−1.72	−1.98	−1.91
B2PLYP/LANL2DZ	−2.40	−1.76	−2.06	−1.93
B2PLYP/SBKJC(*1f*)	−2.46	−1.79	−2.13	−2.02
B2PLYP/MWB60	−2.43	−1.74	−2.09	−1.98
B2PLYP/cc-pVTZ-PP	−2.56	−1.87	−2.19	−2.08
MP2/SBKJC(*1f*)	−2.36	−1.67	−2.20	−2.05

Spin-Orbit Corrections

To apply spin-orbit corrections to the four Au_8 isomers, we replicate the approach described by Johansson *et al.*[5]

Thus, we firstly optimize the isomers with PBEsol/LANL2DZ[6] using the GAMESS-US software package (version Aug. 11 2011). Subsequently, using the program ADF (version 2012.01),[7] we introduce the zeroth-order regular approximation (ZORA)[8] to calculate noncollinear spin-orbit corrections on the four optimized structures. We stick to the following parameters and procedure:[5] all-electron QZ4P basis set, integration accuracy 6.5, TPSS energy[9] calculated via a *post*-SCF procedure on the PBE potential.[10] Data from these calculations are presented in Table S7, where they are compared with the uncorrected PBE/LANL2DZ data presented in the main article.

Table S7: Relative energies of Au_8 **F2**, **F5**, **F6** and **F8** as reported in the main article (optimized with PBE/LANL2DZ; top row), compared to relative energies predicted after applying the spin-orbit correction (bottom row)

Method	**Vertical Detachment Energy / eV**			
	F2	**F5**	**F6**	**F8**
PBE/LANL2DZ	0.000	0.399	0.398	0.534
After spin-orbit correction (ZORA: PBE/QZ4P)	0.000	0.124	0.153	0.280

Assessment of other ECPs and basis sets

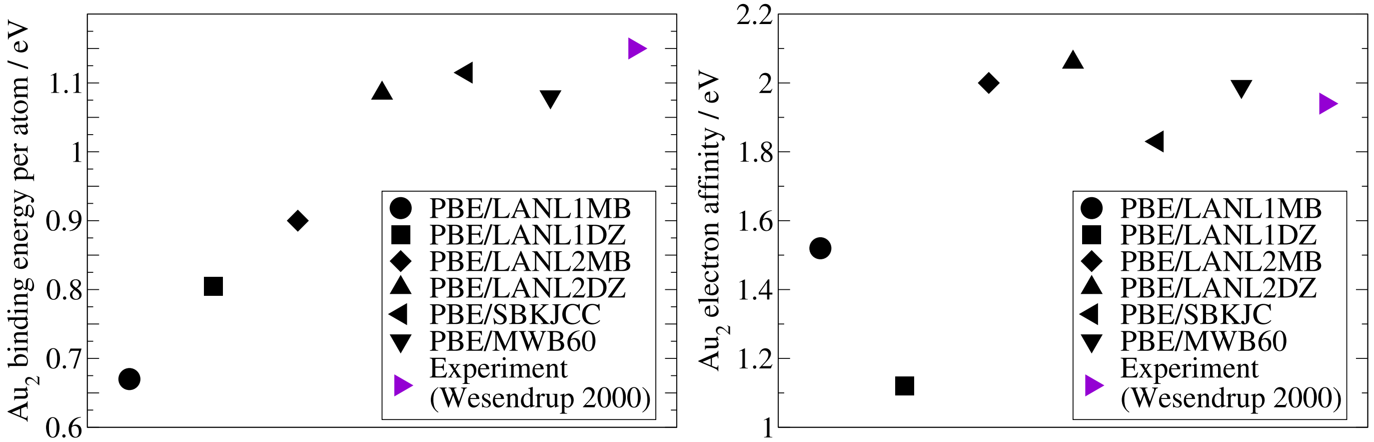

(a) Au_2 binding energy per atom

(b) Au_2 electron affinity

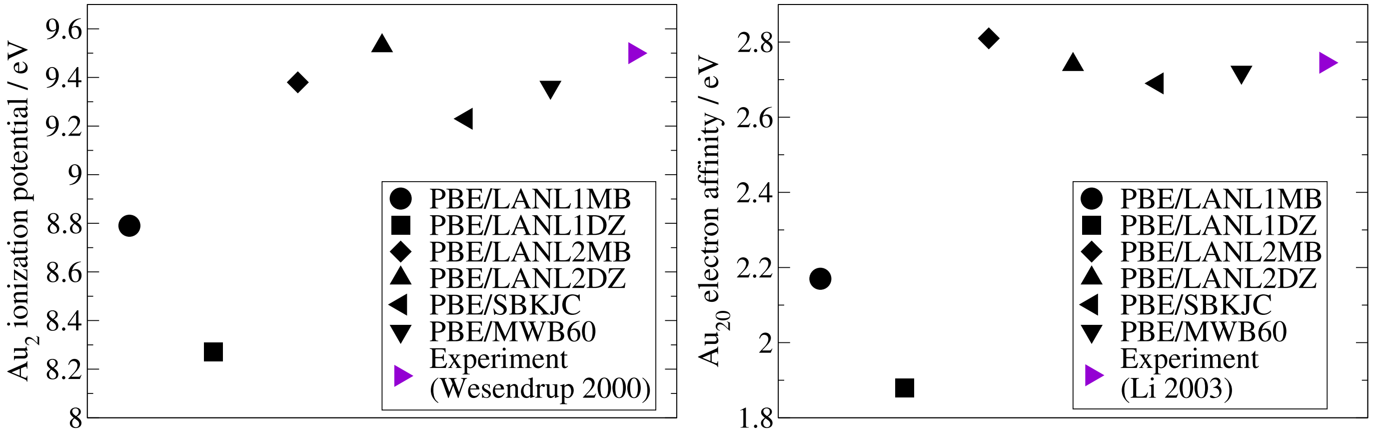

(c) Au_2 ionization potential

(d) Au_{20} electron affinity

Figure S1: Predictions of selected Au_{20} and Au_2 properties by PBE in conjunction with six effective core potentials and basis sets: LANL1MB, LANL1DZ,[11] LANL2MB, LANL2DZ,[12] SBKJC,[13] MWB60.[14] Our own results are compared to corresponding experimental values for Au_2[15] and Au_{20}.[16]

Figure S1 comprises four selected results from our own work (all using the PBE density functional) in which the performance of LANL2DZ is compared with LANL1MB, LANL1DZ,[11] LANL2MB,[12] SBKJC,[13] MWB60[14] as well as with experimental data for Au_2[15] and Au_{20}.[16] Considering the larger sizes and consequent greater computational cost of MWB60 and SBKJC (see Table 1 in the main article), as well as the deviations of LANL1MB, LANL1DZ, LANL2MB from experimental data, we conclude that the LANL2DZ basis set gives the best tradeoff between computational cost and accuracy.

F6 → F5 interconversion with PBE/LANL2DZ and MP2/SBKJC(*1f*)

F5 and **F6** are predicted by PBE/LANL2DZ and MP2/SBKJC(*1f*) calculation to be close in energy (0.001 eV apart in the former case, and 0.025 eV apart in the latter). To confirm that the two are properly separated minima, we have investigated possible **F6** → **F5** interconversion routes along the PBE/LANL2DZ and MP2/SBKJC(*1f*) PESs: this was done *via* successive QST2/QST3 calculations,[17] and subsequent optimisations of the resulting transition states (TSs) along their imaginary frequencies.

Figure S2 illustrates the transition states and intermediates located along the interconversion pathways, and the full energy profiles for the two interconversions are shown in Figure S3.

Different F6 → F5 interconversion pathways found with
PBE/LANL2DZ: MP2/SBKJC(*1f*):

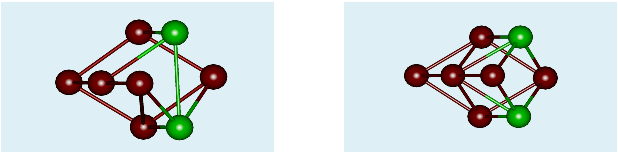

(a) Au$_8$ **F6** (b) Au$_8$ **F6**

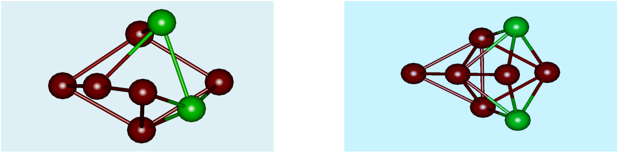

(c) Au$_8$ TS$_{\text{PBEa}}$ (d) Au$_8$ TS$_{\text{MP2a}}$

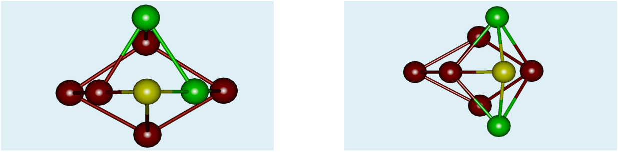

(e) Au$_8$ intermediate (f) Au$_8$ intermediate

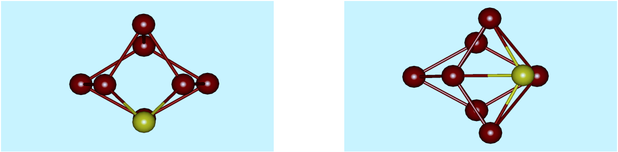

(g) Au$_8$ TS$_{\text{PBEb}}$ (h) Au$_8$ TS$_{\text{MP2b}}$

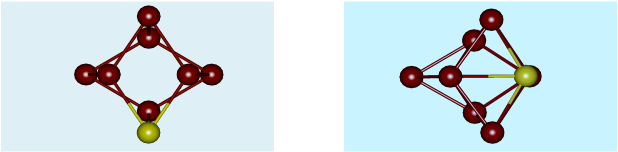

(i) Au$_8$ **F5** (j) Au$_8$ **F5**

Figure S2: Two different potential low energy **F6** → **F5** interconversion routes along: (*left*) the PBE/LANL2DZ PES and (*right*) the MP2/SBKJC(*1f*) PES. Green and yellow atoms are to facilitate visual comparison; some bonds are artificially maintained/deleted for the same reason. Interconversion pathways shown from slightly different angles (*cfr.* different **F5** orientation in (i) and (j)). Energy profiles in Figures S3a and S3b respectively.

The left column of Figure S2 shows the intermediate minimum and two first order transition states encountered on the PBE/LANL2DZ. As indicated in Figure S3a, the first leg of the interconversion involves a 0.163 eV ($6.3k_BT$) 'climb' up to an initial first order $\mathrm{TS_{PBEa}}$ (Figure S2c), before falling to an intermediate minimum nugget (Figure S2e). Its defining characteristic are five gold atoms forming a chevron (>), which can be seen perpendicular to the plane of the page in Figure S2e, with the yellow atom forming its vertex. To complete the rearrangement to **F5**, this minimum has to overcome another 0.033 eV ($1.3k_BT$) barrier, passing through another first order $\mathrm{TS_{PBEb}}$ (Figure S2g), and involving an out-of-plane bending of the chevron's vertex atom.

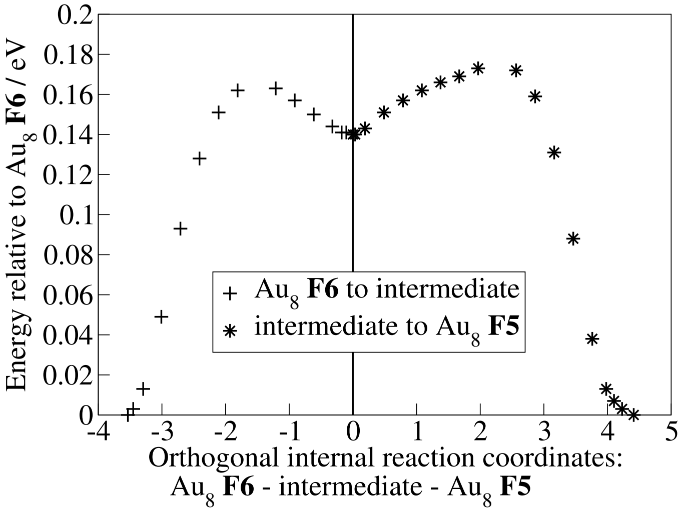

(a) PBE/LANL2DZ interconversion pathway

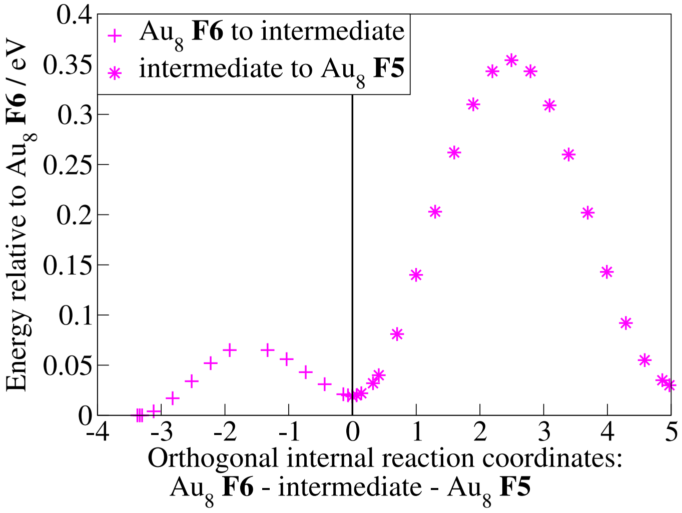

(b) MP2/SBKJC(*1f*) interconversion pathway

Figure S3: Energy profiles for the **F6** → **F5** interconversions shown in Figure S2. Note that internal reaction coordinates for different steps of the interconversion are always orthogonal.

The overbinding effect of MP2 leads to a general destabilization of the PBE/LANL2DZ route: MP2/SBKJC(*1f*) finds that a climb to $\mathrm{TS_{PBEa}}$ would cost 0.308 eV ($11.9k_BT$); we therefore explore another route (Figure S2 right column; Figure S3b), *via* an alternative first order transition state $\mathrm{TS_{MP2a}}$ (Figure S2d), involving a barrier of 0.069 eV ($2.7k_BT$). The intermediate minimum found on this route (Figure S2f) is also characterized by a group of five atoms on the same plane, although arranged as a pentagon rather than a chevron: the yellow atom in Figure S2f forms the pentagon's vertex, and the adjacent green atoms are also part of it.

The most direct route from this intermediate to **F5** is a costly rearrangement of the pentagon's vertex, *via* a

$\mathrm{TS}_{\mathrm{MP2b}}$ (Figure S2h), which is identified as *second* order: this indicates the existence of a lower-energy pathway at the MP2/SBKJC(*1f*) level of theory. We have counter-tested the same route with PBE/LANL2DZ, and were in this case unable to locate a similar intermediate to the one in Figure S2f as a stationary point; we have therefore chosen not to pursue this route further with either method.

As a general overview, we note that there may well exist other energetically cheaper interconversion routes between the two nuggets proceeding *via* a larger number of steps, but given the difference in geometry between Au_8 **F5** and Au_8 **F6**, and considering that the three aligned atoms in **F6** must be somehow 'disrupted' to obtain **F5**, these are unlikely to be easily achievable at 300K.

Coordinates of the Au_8 Isomers Studied

We present in the subsections below the coordinates of the cloverleaf and three nuggets, as optimized by PBE/LANL2DZ. Coordinates are given in the `xyz` format.

F2

```
8
F2
Au 1.621258 -1.379537 1.921772
Au 1.522394 1.194952 1.223213
Au 0.780010 -4.013331 1.397478
Au -1.551385 -1.073272 -2.293803
Au -0.745349 -3.130599 -0.795925
Au 0.095335 -0.496473 -0.271910
Au -0.643427 -5.705690 -0.100139
Au 2.423552 -3.436689 3.422053
```

F5

```
8
F5
Au -0.000181 0.042905 -0.396066
Au 0.000167 2.716109 -1.201121
Au -2.304669 -1.276441 -1.257900
Au 2.303554 -1.277287 -1.258604
Au -1.458597 0.919247 -2.763329
Au 1.457830 0.918725 -2.763757
Au -0.000856 -1.606294 -2.800290
Au -0.000849 0.108836 -5.002732
```

F6

```
8
F6
Au 0.098636 -0.079400 -0.079400
Au 2.800000 -0.155607 -0.155607
Au 5.501364 -0.079400 -0.079400
Au 1.426354 2.383432 0.119701
Au 4.173646 2.383432 0.119701
Au 2.800000 2.568140 2.568140
```

```
Au 1.426354 0.119701 2.383432
Au 4.173646 0.119701 2.383432
```

F8

```
8
F8
Au 0.755741 -1.523318 0.000000
Au 0.755741 1.523317 0.000000
Au 3.495673 -1.831975 0.000000
Au 3.495673 1.831975 0.000000
Au 5.004259 0.000000 1.523317
Au 5.004259 0.000000 -1.523317
Au 2.264327 0.000000 -1.831975
Au 2.264327 0.000000 1.831975
```

References

[1] M. Diefenbach and K. S. Kim, *J. Phys. Chem. B*, 2006, **110**, 21639–21642.

[2] C. Jackschath, I. Rabin and W. Schulze, *Ber. Bunsen-Ges.*, 1992, **96**, 1200–1204.

[3] H. Häkkinen, B. Yoon, U. Landman, X. Li, H. J. Zhai and L. S. Wang, *J. Phys. Chem. A*, 2003, **107**, 6168–6175.

[4] K. J. Taylor, C. L. Pettiettehall, O. Cheshnovsky and R. E. Smalley, *J. Chem. Phys.*, 1992, **96**, 3319–3329.

[5] M. P. Johansson, A. Lechtken, D. Schooss, M. M. Kappes and F. Furche, *Phys. Rev. A*, 2008, **77**, 053202–053208.

[6] J. P. Perdew, A. Ruzsinszky, G. I. Csonka, O. A. Vydrov, G. E. Scuseria, L. A. Constantin, X. Zhou and K. Burke, *Phys. Rev. Lett.*, 2008, **100**, 136406–136409.

[7] G. te Velde, F. M. Bickelhaupt, E. J. Baerends, C. Fonseca Guerra, S. J. A. van Gisbergen, J. G. Snijders and T. Ziegler, *J. Comput. Chem.*, 2001, **22**, 931–967.

[8] E. van Lenthe, E. J. Baerends and J. G. Snijders, *J. Chem. Phys.*, 1994, **101**, 9783–9792.

[9] J. Tao, J. P. Perdew, V. N. Staroverov and G. E. Scuseria, *Phys. Rev. Lett.*, 2003, **91**, 146401–146404.

[10] J. P. Perdew, K. Burke and M. Ernzerhof, *Phys. Rev. Lett.*, 1996, **77**, 3865–3868.

[11] P. J. Hay and W. R. Wadt, *J. Chem. Phys.*, 1985, **82**, 270–283.

[12] P. J. Hay and W. R. Wadt, *J. Chem. Phys.*, 1985, **82**, 299–310.

[13] W. J. Stevens, M. Krauss, H. Basch and P. G. Jasien, *Can. J. Chem.*, 1992, **70**, 612–630.

[14] D. Andrae, U. Häußermann, M. Dolg, H. Stoll and H. Preuß, *Theor. Chim. Acta*, 1990, **77**, 123–141.

[15] R. Wesendrup, T. Hunt and P. Schwerdtfeger, *J. Chem. Phys.*, 2000, **112**, 9356–9362.

[16] J. Li, X. Li, H. J. Zhai and L. S. Wang, *Science*, 2003, **299**, 864–867.

[17] C. Peng, P. Y. Ayala, H. B. Schlegel and M. J. Frisch, *J. Comput. Chem.*, 1996, **17**, 49–56.